ACS OMEGA

Open Access

http://pubs.acs.org/journal/acsodf

Article

High-Performance 3D Nanostructured Silver Electrode for Micro-Supercapacitor Application

Ana Silvia González, Javier García, Victor Vega, Rafael Caballero Flores, and Victor M. Prida*

Cite This: *ACS Omega* 2023, 8, 40087−40098

Read Online

ACCESS | Metrics & More | Article Recommendations | Supporting Information

ABSTRACT: In the current energy crisis scenario, the development of renewable energy forms such as energy storage systems among the supercapacitors is an urgent need as a tool for environmental protection against increasing pollution. In this work, we have designed a novel 3D nanostructured silver electrode through an antireplica/replica template-assisted procedure. The chemical surface and electrochemical properties of this novel 3D electrode have been studied in a 5 M KOH electrolyte. Microstructural characterization and compositional analysis were studied by SEM, energy-dispersive X-ray spectroscopy, XRD technique, and Kripton adsorption at −198 °C, together with cyclic voltammetry and galvanostatic charge−discharge cycling measurements, Coulombic efficiency, cycle stability, and their leakage current drops, in addition to the self-discharge and electrochromoactive behavior, were performed to fully characterize the 3D nanostructured electrode. Large areal capacitance value of 0.5 F/cm^2 and Coulombic efficiency of 97.5% are obtained at a current density of 6.4 mA/cm^2 for a voltage window of 1.2 V (between −0.5 and 0.8 V). The 3D nanostructured silver electrode exhibits excellent capacitance retention (95%) during more than 2600 cycles, indicating a good cyclic stability. Additionally, the electrode delivers a high energy density of around 385.87 μWh/cm^2 and a power density value of 3.82 μW/cm^2 and also displays an electrochromoactive behavior. These experimental results strongly support that this versatile combined fabrication procedure is a suitable strategy for improving the electrochemical performances of 3D nanostructured silver electrodes for applications as micro-supercapacitors or in electrochemical devices.

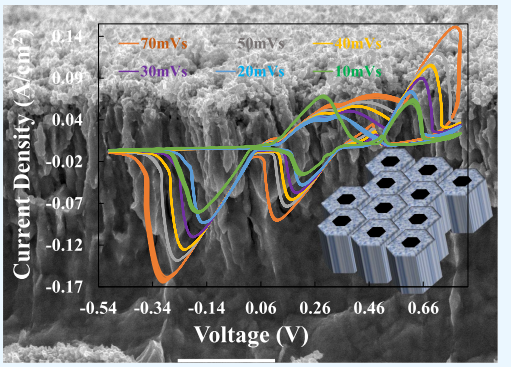

1. INTRODUCTION

One of the highest priorities of energetic plan action that affects worldwide concerns the transformation to renewable energies and optimized management of resources in order to reduce the carbon fingerprint and mitigate climate change. This transformation not only pretends to substitute all energy sources with renewables without endangering the natural development of the society. In fact, it pretends an electrification of as many economical areas such as automotive or heating and cooling industries among others. Considering electricity as the primary energy source, it is becoming increasingly more important to find new and more efficient ways of electrical energy storage. Many of the limits associated with batteries and their declining credibility as storage solutions have led to alternative energy markets predicting supercapacitors to replace batteries entirely in the middle term.[1,2]

Supercapacitors, also known as ultracapacitors or electrochemical capacitors, exhibit outstanding properties for use as energy storage systems due to their high power density, fast charge−discharge rates, and excellent cycle stability, plus other qualities. They can be divided into two large groups: electric double-layer capacitors (EDLCs) and pseudocapacitors.[3] EDLCs employed their very thin double-layer structure to store the electrical charges, while pseudocapacitors store the electrical charges through fast and reversible redox reactions. For this, the pseudocapacitors show much higher capacitance compared with the capacitive capability of double-layer capacitors where a much lower degree of electron transfer occurs,[4,5] showing that they are considered as an excellent source of potential candidates like energy storage devices in many research areas such as in energy sources for portable devices, memory power sources, energy power recovery and regeneration systems, or electrical energy distribution machines and storage devices.[6] Nowadays, investigations about pseudocapacitors are addressed to the discovery of new advanced nanostructured materials presenting high effective surface areas or different morphologies with enhanced energy densities or improving the capacitance of pseudocapacitors. In the context of the analysis about which materials could serve as optimal electrodes for pseudocapacitors, four key factors need to be taken into consideration: (1) high

Received: April 3, 2023
Accepted: September 29, 2023
Published: October 17, 2023

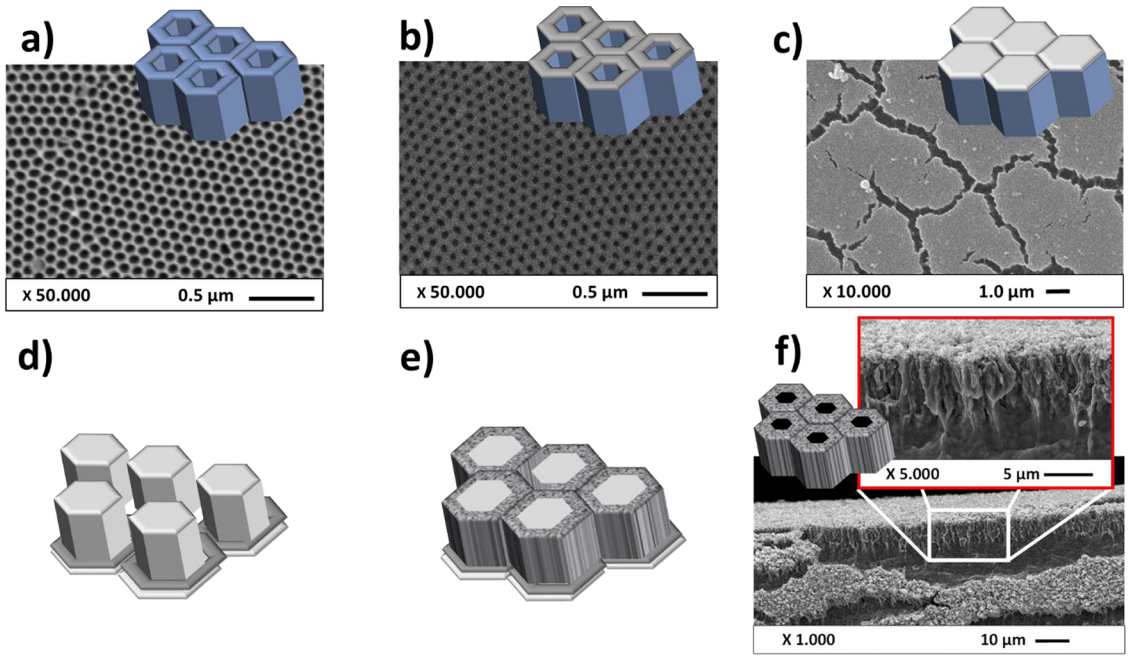

Figure 1. Schematic picture of the subsequent processes for the fabrication of a 3D nanostructured silver electrode: nanoporous alumina template grown during the anodization procedure (a); vacuum thermal evaporation of the Ag seed layer on the top surface of the AAO template forming the nanostructured Ag antidot film platform (b); infiltration of poly(methyl methacrylate) (PMMA) and chloroform (3 g of PMMA in 50 mL of chloroform) solution inside the nanoholes of Ag antidot film platform (c); Al- and Al_2O_3-selective chemical etchings (d); silver electrodeposition for the replicated template (e); and final replica of the 3D nanostructured silver electrode (f).

surface area for the redox reactions, (2) doping of the materials to increase the redox state and their conductivity, (3) a wide potential window, and (4) a high charge/discharge rate.[7−11] About the different materials, conducting polymers and transition-metal oxides can be found to meet these requirements; however, metal oxides are generally considered the main candidates that can be used as electrode materials in supercapacitors because of the wide variety of oxidation states that allows for redox charge transfer, together with other excellent properties to be used as electrodes in supercapacitor devices for energy storage applications (such as high specific surface area, high conductivity, abundant reserves, environmental geniality, etc.). Therefore, among the different metal oxides, the most widely used oxides as electrodes for pseudocapacitors include tin oxide (SnO_2), ruthenium oxide (Ru_2O), cobalt oxide (Co_3O_4), nickel oxide (NiO), iron oxide (Fe_2O_3), vanadium oxide (V_2O_5), copper oxide (CuO), tungsten oxide (WO_3), iridium oxide (IrO_2), molybdenum oxide (MoO_3), manganese oxide (MnO_2), and so forth.[12−14] Among these metal oxides, ruthenium oxide has attracted a lot of attention due to its high conductivity, good thermal stability, and excellent electrochemical performance; however, its high environmental toxicity and high cost hinder its commercialization as an electroactive material for supercapacitor applications.

Consequently, current novel investigations are being done in search of other alternatives for electrode materials in pseudocapacitors. Among these alternatives, silver generates high interest as it exhibits an electrochemical behavior close to that of ruthenium oxide, is cheaper than ruthenium oxide, and is more environmentally sustainable.[15,16] Also, silver in its different oxidation states (AgO, Ag_2O, and Ag_2O_2) is more conductive than other transition-metal oxides investigated for pseudocapacitor applications and has more ability to change and adopt different oxidation states (+1, +2), providing the energy storage ability. Furthermore, from the electrochemical perspective, silver is very reactive and forms different oxide phases such as AgO, Ag_3O_4, Ag_4O_3, Ag_2O_3, and Ag_2O, where Ag_2O is the most stable among them.[17−22] In addition, silver has been used in previous studies as a component of electrodes; also, silver nanowires are commonly used in flexible and wearable electronic devices. Nanocomposites of silver nanoparticles with graphene, carbon nanotubes, metal oxides, or conducting polymers have been tested for their use in several energy storage applications. Also, silver has been reported to be used with metal oxides including MnO, NiO, CuO, and Co_3O_4, where the presence of silver alleviates problems associated with the low electrical conductivity of metal oxides.[23−31] Therefore, the main objective of this work deals with investigating the excellent qualities displayed by silver for its use like an electrode for pseudocapacitors because this novel research line possesses currently a real interest from a scientific point of view.

Several fabrication methods can be employed to synthesize metal oxides for supercapacitor electrodes with different morphologies. Some of these methods include screen printing, hydrothermal, electrophoretic deposition, chemical precipitation, solvothermal, chemical bath deposition, microwave-assisted deposition, and sonochemical methods.[32−36] In addition, the use of nanostructured templates in combination with the previous methods offers the possibility of designing new nanostructured electrodes with high surface areas and optimized morphologies, where the interface contact between the electrode and electrolyte can be promoted. Furthermore, the development of a nanoporous structure of the electrode allows the liquid electrolyte to easily diffuse into the electrode material, thus increasing its specific surface area, which results in huge interest for applications in supercapacitors, sensors, catalysis, lithium-ion batteries, and adsorption.[37,38] In a

https://doi.org/10.1021/acsomega.3c02235
ACS Omega 2023, 8, 40087−40098

previous work by Zhao et al., a self-supported metallic MnO_2@Ni-nanostructured electrode was developed by following a replica/antireplica synthesis technique based on nanoporous anodic aluminum oxide (AAO) templates, where the highly oriented nanoporous structure of the former AAO templates was demonstrated to be highly desirable for the metallic electrodes in supercapacitor applications.[39] Also, the recent work made by Brzózka et al. compares between the electrocatalytic properties of nanostructured metallic electrodes made by highly ordered arrays of Ag nanowires and hemispherical Ag nanocups, which were fabricated through the AAO template-assisted electrochemical deposition method in the case of Ag nanowire arrays, or the metallic sputtering deposition technique for the hexagonal ordered arrangement of Ag nanohemispheres.[40] Taking into account that surface area and morphology have a major influence on the capacity of the electrode material, it becomes important to implement a fabrication process able to provide nanostructured materials with high surface area, uniform pore size, and highly ordered parallel alignment, together with well-controlled porosity, in order to achieve excellent performance as electrochemical capacitor systems.[41−45]

In this work, we report on a novel strategy to prepare 3D nanostructured silver electrodes (3D-NSEs) for supercapacitors using a fast, facile, and cost-effective antireplica/replica process where we have used AAO as precursor templates for the fabrication of electrodes. The electrochemical and surface chemical properties of the 3D nanostructured silver electrode were systematically studied in a 5 M KOH electrolyte. The surface morphologies, capacitive properties, and redox couples of the 3D-NSEs were characterized by SEM, XRD, Kripton adsorption at −198 °C, cyclic voltammetry (CV), galvanostatic charge−discharge cycling measurements, Coulombic efficiency, cycle stability, working voltage, self-discharge, and electrochromoactive behavior. The fabricated 3D-NSE exhibited a high areal capability of 0.5 F/cm^2 and 97.5% Coulombic efficiency at a current density of 6.4 mA/cm^2 and excellent charge−discharge cycling stability with 95% capacitance retention after 2600 cycles. Also, the electrode delivers a high energy density of around 385.87 μWh/cm^2 and a power density value of 3.82 μW/cm^2 and also displays an electrochromoactive behavior. These results suggest that this 3D-NSE presents excellent qualities for its use in energy storage devices such as supercapacitors and secondary batteries.

2. EXPERIMENTAL PROCEDURE

2.1. Synthesis of 3D Nanostructured Silver Electrode. The 3D-NSE has been fabricated by following an antireplica/replica procedure employing nanoporous AAO as precursor templates.[39,40,44] This fabrication method consists of a series of processes, where the first one corresponds to the preparation of porous alumina membrane by a two-step electrochemical anodization process.[46] The additive fabrication process flow is schematized in Figure 1a−f. The nanoporous AAO templates have been fabricated by employing the well-known two-step anodization (mild anodization) process using 0.3 M oxalic acid as the electrolyte of the anodization bath with a pH of 0.5.[39,40,44] High-purity aluminum discs (Al 99.999%) were used as source substrates for the fabrication of the nanoporous AAO membrane (0.5 mm in thickness and 25 mm in diameter). Before the anodization process, the aluminum substrates were first cleaned by sonication in isopropanol and ethanol and after this electropolished in a mixture of $HClO_4$ and ethanol (25:75) to smoothen the surface for 300−500 s at 5 °C under a voltage of 20 V applied between the foil and a platinum counter-electrode. After that, the Al substrates were cleaned with distilled water (resistivity value: 18.2 MΩ/cm). Subsequently, the foils were first anodized in 0.3 M oxalic aqueous solution under a voltage of 40 V at a temperature of 1−3 °C for 24 h. Then, the alumina grown during the first anodization process was chemically etched by a mixed aqueous solution of 0.2 M CrO_3 and 0.6 M H_3PO_4 at 35 °C for 24 h. The second anodization step was conducted under similar circumstances as the first one but lasting for 1 h, leading to a highly hexagonally ordered nanopore arrangement in the AAO template. Afterward, the diameter of the former nanopores was enlarged through a pore-widening process in phosphoric acid (5% in volume) at 30 °C for 35 min. After this chemical treatment, the final pore diameter of nanoporous AAO samples is estimated to be around 70 nm (Figure 1a).

In order to create a working electrode for Ag electrodeposition, a 50 nm thick Ag seed layer was deposited by vacuum thermal evaporation process, which involves the evaporation of the metal on the top surface of the nanoporous anodic alumina membranes used as patterned templates,[47] thus forming a nanostructured silver antidot film platform (Figure 1b).

Subsequently, the nanoholes of the Ag antidot film layer were then filled at room temperature by a solution of poly(methyl methacrylate) (PMMA) and chloroform (3 g of PMMA in 50 mL of chloroform) (Figure 1c). Following this, two selective chemical etchings were carried out to remove the Al substrate and the alumina layer. An aqueous mixture of 50 mL of HCl (37%) and 0.3 M $CuCl_2$ was employed to perform chemical etching and partially remove the Al substrate, by exposing an area of around 1.8 cm^2 of the AAO backside. The alumina layer was further removed by immersing the samples in an acidic solution of 0.2 M CrO_3 and 0.6 M H_3PO_4 (Figure 1d). Then, the metallic silver antidot film platform was electroplated using the silver nanolayer as an electrode in a commercial silver electrolyte (silver volume, 28.7 g/L) bath under a voltage of −1.7 V for 6 h (Figure 1e), employing a two-electrode electrochemical cell, performed at room temperature. After the subsequent removal of the polymer by immersion in chloroform, a 3D nanostructured silver electrode was finally obtained (Figure 1f). Thus, it can be seen from Figure 1f that the 3D nanostructured silver electrode shows an irregular columnar nanostructure grown with roughness along the sides of the columns. It is because of the way in which silver is electroplated into the nanopatterned polymer template, where the irregular and rough columnar shape of Ag oxide nanostructure tries to replicate the nanopatterning of the former alumina template.

2.2. Morphological and Microstructural Characterization and Chemical Analysis of 3D-NSEs. The structure and morphology of the 3D nanostructured silver electrode have been first investigated by SEM in a JEOL 6610LV microscope, equipped with an Oxford INCA EDX microanalysis system. The SEM system is fitted with a tungsten filament electron gun, which operates at an acceleration voltage of 20 kV. Top and bottom surface views and cross-sectional images of the samples were obtained. The chemical characterization of the 3D-NSE was performed by local EDX analysis, which allows us to determine the elemental chemical distribution on the sample.

https://doi.org/10.1021/acsomega.3c02235
ACS Omega 2023, 8, 40087−40098

XRD were also performed as a complementary technique to analyze the crystallographic microstructure of the sample. The XRD patterns of the 3D-NSE were obtained by an X-ray powder diffractometer with an XPERT-PRO diffractometer system within the angle range of $20° < 2\theta < 90°$.

The effective surface area of the electrode sample was estimated accordingly by krypton (Kr) gas adsorption measurements carried out at 75 K (−198 °C) in an ASAP2420 volumetric apparatus. Previous to this analysis, the sample was degassed at 150 °C for 15 h under vacuum. The motivation for using this characterization method is that the krypton adsorption method of measurement is much more sensitive at these temperatures and can be applied to assess surface areas down to at least 0.05 m^2, so it is considered a standard method for performing low surface area analysis.[48]

2.3. Electrical Properties of Nanostructured Ag Electrode. *2.3.1. Cyclic Voltammetry.* The cyclic voltammetry (CV) measurements performed in the 3D-NSE have been carried out with a Potenciostat AMEL instrument (Model 7050). Ten sequential cycles were programmed at the different scan rates of 10, 20, 30, 40, 50, and 70 mV/s in a potential window ranging from −0.5 V up to 0.8 V versus the Ag/AgCl reference electrode. The areal capacitance is proportional to the integral of the CV curve and can be determined from the charge value Q. Thus, Q is identified as the difference between the area under the charge curve and the area under the discharge curve data ranging between the upper and lower limits of the potential window.

Thus, the areal capacitance can be obtained from eqs 1−3:[49−56]

$$\left(Q = \int I \cdot \mathrm{d}t;\ t = \frac{V}{\mathrm{v}}\right) \tag{1}$$

$$Q = \frac{1}{\mathrm{v}} \int I \cdot \mathrm{d}V \tag{2}$$

$$\left(C = \frac{Q}{a \cdot \Delta V};\ C = \frac{\int I \cdot \mathrm{d}V}{\mathrm{v} \cdot a \cdot \Delta V}\right) \tag{3}$$

where I is the current (A), t is the time (s), V is the voltage (V), v is the scan rate parameter (V/s), C is the areal specific capacitance (F/cm^2), a is the surface area of the device in the single electrode in cm^2, and it is fixed at 1 cm^2 for this study, and Q is the charge/discharge value (C).

2.3.2. Charging/Discharging Measurements. The charging/discharging measurements of the nanostructured electrode were carried out by means of a source measure unit (SMU) KEITLEY (Model 2010) with a current density of 6.4 mA cm^{-2} and a voltage window of 1.2 V. From the charging/discharging measurements, the specific capacitance value was calculated according to eq 4:[49−56]

$$C = (I \cdot t_\mathrm{d})/(a \cdot \Delta V) \tag{4}$$

where C (F/cm^2) is the areal specific capacitance, I (A) is the discharge current, t_d (s) is the discharging time, a (cm^2) is the surface area of the device in the single electrode given in cm^2 which is fixed at 1 cm^2 in this study, and ΔV (V) is the voltage window for discharge.

2.3.3. Coulombic Efficiency and Cycling Stability. The Coulombic efficiency of the 3D-NSE was also measured in an SMU KEITLEY system (Model 2410). The Coulombic efficiency can be calculated through the following equation:[49−56]

$$\eta = \frac{t_\mathrm{d}}{t_\mathrm{c}} \tag{5}$$

where t_c and t_d represent the charge and discharge times, respectively.

The leakage current (LC) of supercapacitors corresponds to the tiny current that flows when the rated voltage continues to be applied to the capacitor. The leakage current is equivalent to the charging current required to maintain the supercapacitor at the specified voltage value. It is measured in amperes (A). The leakage current was measured in a Potenciostat AMEL instrument (Model 7050) by keeping the supercapacitor at a constant voltage value of 0.7 V and the measured time interval for 2 h.

When the device has a high internal resistance and the charging source is disconnected from the supercapacitor, the device can start losing its charge. This is called the self-discharge characteristic that consists of a voltage drop of the charged capacitor after a time period with no load condition. The self-discharge of the electrode was measured in a SMU KEITLEY instrument (Model 2400). The electrode was charged at 0.7 V, and the measured time was 5 h.

The motivation for measuring the leakage current and self-discharge of the supercapacitor is due to the importance for practical applications of the device.

To calculate the energy density (E_d) and power density (P_d) of the samples, eqs 6 and 7 were used:[49−56]

$$E_\mathrm{d} = \frac{1}{2} C \cdot V^2 \tag{6}$$

$$P_\mathrm{d} = \frac{E_\mathrm{d}}{t_\mathrm{d}} \tag{7}$$

where C (0.5 F/cm^2) is the areal specific capacitance from charging/discharging measurements, E_d is the energy density, P_d is the power density, t_d is the discharge time, and V is the potential window of the three-electrode measurement system (1.2 V).

2.4. Optical Characterization of Nanostructured Silver Electrodes. Finally, the electrochromoactive behavior of 3D-NSEs was analyzed. For this study, we apply a staircase voltage ramp across the electrode to induce redox reactions, therefore modifying the energy bands that interact with the visible light and thus changing the surface color of the electrode. In this particular case, the samples were analyzed by measuring the reflected light on the sample as a function of the applied potential. As a photometric measurement of luminous intensity, the luminance of the electrodes has been calculated using an RGB (red, green, and blue) code 8:[57]

$$\mathrm{Luminance}(\%) = 100 \times (0.2126 \cdot \mathrm{R} + 0.7152 \cdot \mathrm{G} + 0.0722 \cdot \mathrm{B}) \tag{8}$$

Such a color change experienced by the 3D-NSE during the charging/discharging measurements can be an excellent indicator of proper functioning of the nanostructured Ag electrode.

3. RESULTS AND DISCUSSION

3.1. Microstructure and Chemical Analysis of 3D-NSEs. Figure 2a,b shows the SEM images corresponding to the

https://doi.org/10.1021/acsomega.3c02235
ACS Omega 2023, 8, 40087−40098

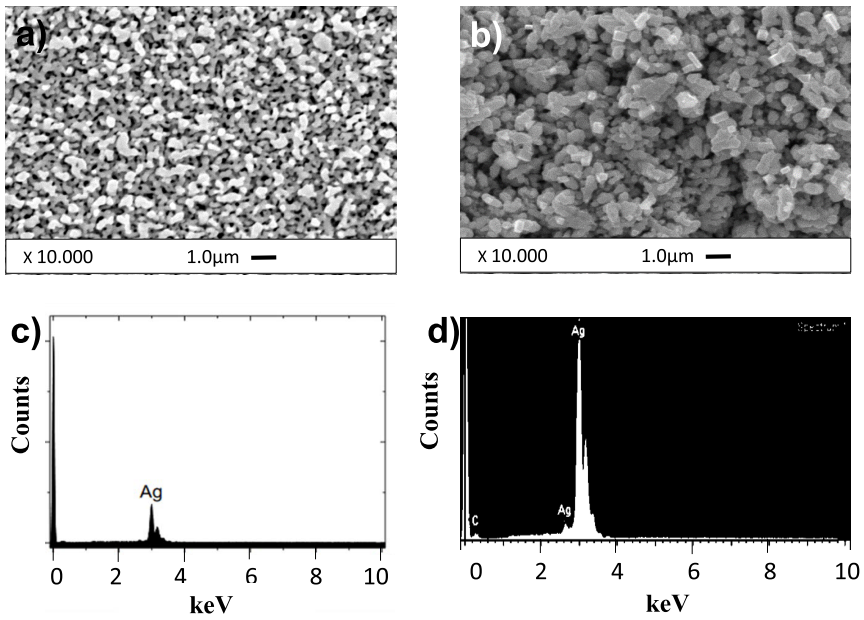

Figure 2. SEM top-view surface images corresponding to the 3D-NSE before (a) and after (b) the stability tests. EDX microanalysis was performed on the top surface of the 3D-NSE before (c) and after (d) the stability tests.

3D-NSE with nanohole structure by replicating the former nanoporous AAO template, before (Figure 2a) and after (Figure 2b) the stability tests. From these SEM images it is possible to see that the 3D-NSE structure hardly changed after its performance. In order to determine the chemical composition of the 3D-NSE, EDX microanalysis was performed on the top surface of the sample before and after the stability tests. Figure 2c,d shows the EDX profile where only the presence of Ag has been detected, which confirms the successful fabrication approach for the nanostructured Ag electrodes and that the chemical composition does not change after the stability tests.

The XRD patterns provide information about the crystallographic microstructure of the 3D-NSE before and after the stability tests (Figure 3). According to the literature consulted,

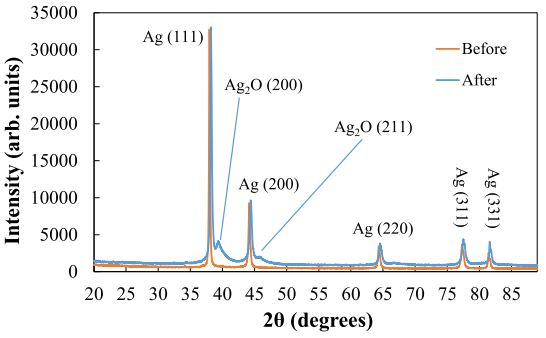

Figure 3. XRD patterns of the 3D-NSE before (red) and after (blue) the stability tests.

the XRD peaks appeared at 2θ of 37.99°, 44.2°, 64.4°, 77.4°, and 81.7°, which can be attributed to (111), (200), (220), (311), and (331) crystallographic planes of face-centered cubic (fcc) silver crystals, respectively, and XRD peaks at 2θ of 39.57° and 46.38° can be attributed to a small portion of cubic crystallographic phase corresponding to Ag_2O, indicating that after the stability tests there may be some remnants of silver oxide.[58−60] From the XRD results, it was found that the 3D-NSE possesses a crystallographic plane of face-centered cubic (fcc) structure and that the preferred growth orientation of the 3D-NSE is fixed at the (111) direction.

The effective surface area of the 3D-NSE sample was estimated by a Krypton gas adsorption isotherm measured at 75 K (−198 °C), which is shown in Figure 4. The specific

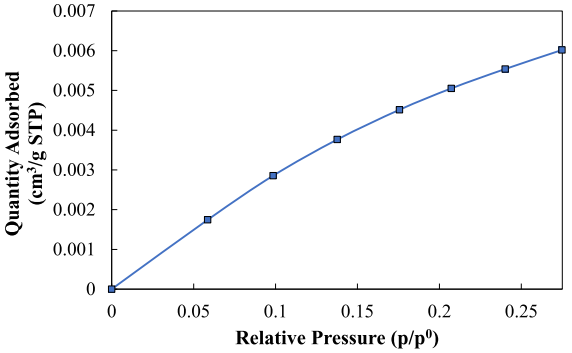

Figure 4. Krypton gas adsorption isotherm measured at 75 K for the 3D-NSE sample.

surface area was calculated by applying the Brunauer−Emmet−Teller equation in the relative pressure range between 0.1 and 0.3.[48] The obtained value for the specific surface area of the 3D-NSE is 0.0344 ± 0.0014 m^2/g. Based on the results obtained through the krypton gas adsorption isotherms measured at 75 K, it is clear that the entire surface area of the 3D-NSE device in the single electrode in cm^2 is potentially reactive to the reversible redox reactions, which are the typical reactions that take place in these kinds of supercapacitor electrodes, in contrast to the double-layer electrodes where the double-layer charging is related to the capacitive-like nature of the electrode/electrolyte interface.

3.2. Electrochemical Properties of 3D-NSEs. To investigate the electrochemical properties of the nanostructured electrode, CV experiments were performed. The CV

https://doi.org/10.1021/acsomega.3c02235
ACS Omega 2023, 8, 40087−40098

curves were measured in 5 M KOH electrolyte at different scan rates (10, 20, 30, 40, 50, and 70 mV/s), with the potential window ranging from −0.5 V up to 0.8 V. The electrochemical measurements were performed in a three-electrode electrochemical cell, with the 3D nanostructured silver electrode as the working electrode, a Pt foil as the counter electrode, and Ag/AgCl as the reference electrode.

The motivation for employing the Pt foil as a counter electrode is due to the platinum being commonly employed as a counter-electrode material. The use of platinum as an electrode is due to its excellent properties, such as inertness and nonreactiveness, resistance to acid attack and nonirritants, together with a long-lasting electrode, and so forth.[61]

With respect to the reference electrode, Ag/AgCl is a widely used reference electrode because it is simple, inexpensive, very stable, and nontoxic; also, it works in a wide temperature range (other reference systems like the Hg/Hg_2Cl_2 electrode can be used only at temperatures no higher than 60−70 °C). In addition, it is a nonpolarizable DC reference electrode because it has a well-defined DC potential not very dependent on the DC current flow.[62]

Figure 5a shows the CV curves of the 3D-NSE. From the CV analysis, it is possible to see how all curves exhibit different

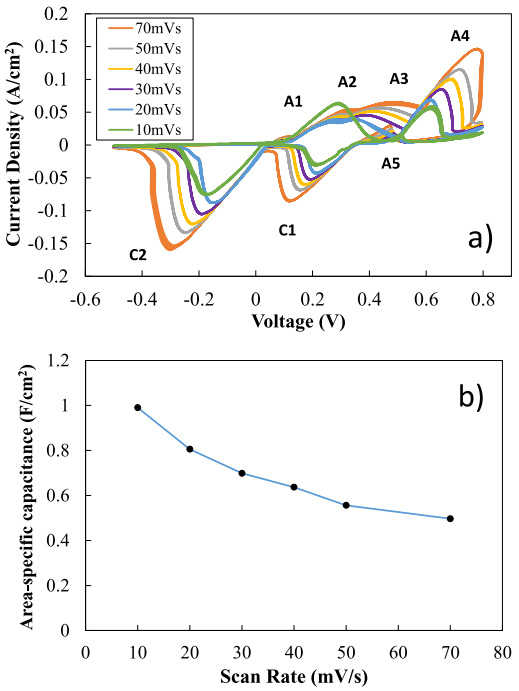

Figure 5. CV curves of the 3D-NSE measured in 5 M KOH aqueous solution at different scan rates within a potential window ranging from −0.5 V up to 0.8 V with respect to the Ag/AgCl reference electrode (a); variation of the area-specific capacitance with the scan rate (b).

redox peaks, which are responsible for the pseudocapacitance behavior exhibited by the 3D-NSE, because the areal capacitance is proportional to CV areas (eqs 1−3). However, it can be seen from the CV curves how the characteristic capacitance of the 3D-NSE is very different from the typical ideal rectangular shape shown by the electric double-layer capacitors.[37] If we analyze Figure 5a, it is possible to see four anodic current peaks (two minor ones (A_1 and A_2) and two major ones (A_3 and A_4)), in the anodic section of the CV curve, prior to the oxygen evolution potential. However, in the reverse potential scan, we can see an activated anodic current peak (A_5) and two cathodic contributions (C_1 and C_2), prior to the hydrogen evolution potential.[63,64]

The A_1 anodic peak may be associated with the electrodissolution of Ag into $[Ag(OH)_2^-]$ on the basis of diffusion of soluble $[Ag(OH)_2]$ and of adsorption and desorption of OH^-[63,64] by following the respective reactions 9 and 10:

$$Ag + 2OH^-_{ads} \leftrightarrow [Ag(OH)_2]^-_{ads} + e^- \quad (9)$$

$$[Ag(OH)_2]^-_{ads} \leftrightarrow [Ag(OH)_2]^-_{aq} \quad (10)$$

The A_2 anodic peak may be associated with the electroformation of a monolayer of Ag_2O coming from the precipitation of $[Ag(OH)_2]$ from its supersaturated solution at the electrode surface.[40,41] Furthermore, the A_3 anodic current peak can be ascribed to the nucleation and growth of a Ag_2O multilayer following the chemical reaction 11:[63,64]

$$2Ag + 2OH^- \leftrightarrow Ag_2O + H_2O + 2e^- \quad (11)$$

Finally, the A_4 anodic peak may be associated with the electrooxidation of Ag_2O and the formation of AgO in accordance with the following chemical reaction 12:[63,64]

$$Ag_2O + 2OH^- \leftrightarrow 2AgO + H_2O + 2e^- \quad (12)$$

On the other hand, the A_5 anodic peak appeared at the reverse scan that has been reported in the same potential range of the A_3 peak, which can be associated with the continuous nucleation and growth of an Ag_2O film as a result of electrooxidation of the basal Ag metal.[63,64] Paying attention to the cathodic section of the CV studied, it is possible to observe two reversible reactions. First, the C_1 cathodic peak could be ascribed to the electroreduction of AgO into Ag_2O, indicating that this peak is conjugated to the A_4 anodic peak, according to the chemical reaction 13:[63,64]

$$2AgO + H_2O + 2e^- \leftrightarrow Ag_2O + 2OH^- \quad (13)$$

Finally, the more negative C_2 cathodic peak can be associated with the processes involved in the electroreduction of Ag(I) oxygen species into metallic Ag.[64]

In Figure 5a, it becomes noticeable that with the increasing sweeping rates, the anodic and cathodic potential peaks shift in the more anodic and cathodic directions, respectively, thus decreasing the capacitance. The lower capacitance for high scan rates (Figure 5b) is a consequence of the migration and diffusion of electrolyte ions restricted at the surface of the electrode, whereas bulk diffusion occurs at lower scan rates, yielding larger capacitance values.[65,66] This electrochemical behavior indicates the presence of pseudocapacitance, where the electron transfer process of the redox reactions is very dependent on the voltage scan rate, caused by the polarization in the electrode material. The shapes of the CV curves reveal that the characteristic capacitance is well distinguished from that of the electric double-layer capacitance, where the CV curve is normally close to an ideal rectangular shape.[67−69]

Galvanostatic charge−discharge (GCD) curves of the 3D-NSE are shown in Figure 6a. The cycling performances of the samples were estimated at a current density of 6.4 mA cm^{-2}. The GCD curve exhibited a symmetric shape, which is indicative of an excellent reversibility behavior and an optimal capacitive behavior of the material.[70]

https://doi.org/10.1021/acsomega.3c02235
ACS Omega 2023, 8, 40087−40098

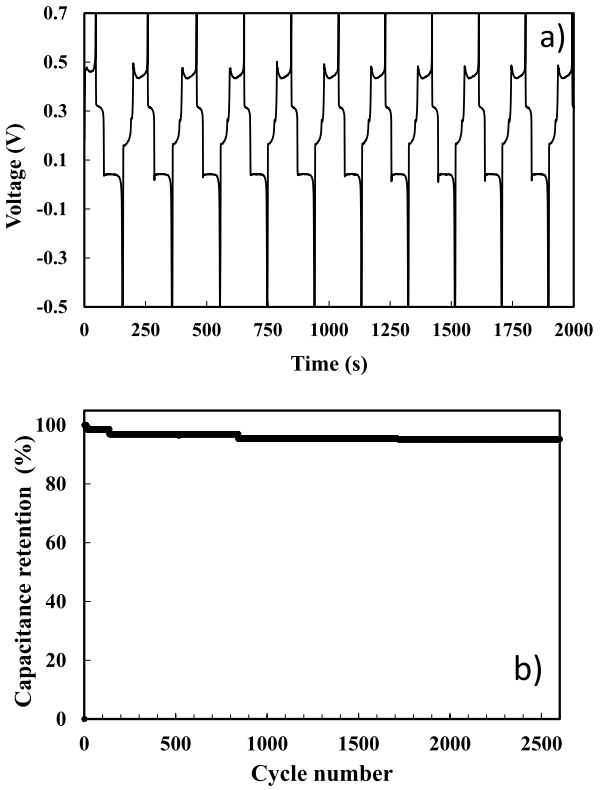

Figure 6. GCD curves of the 3D-NSE at a current density of 6.4 mA cm^{-2} (a) and cycle performance of the 3D-NSE during 2600 GCD cycles (b).

Also, the nearly symmetric potential−time relation of the galvanostatic charge/discharge curves implies low polarization value of the nanostructured Ag electrode and high charge−discharge Coulombic efficiency from it,[71,72] and the charge−discharge platforms are also consistent with the redox peaks that can be observed in the CV curves, indicating that redox reactions occur during the energy storage and release processes.[73−75]

Base on the obtained GCD curves, it is possible to calculate the Coulombic efficiency, which was approximately 97.5%, demonstrating the high efficiency of the fabricated 3D-NSE. Additionally, it is possible to show from Figure 6b that the 3D-NSE also delivers good cycling stability with a capacitance retention of 95% and that no significant areal capacitance is lost after 2600 cycles. Finally, the areal capacitance calculated from the charge/discharge curves (eq 4) reaches a high value of 0.5 F/cm^2, confirming that the 3D-NSE exhibits a high areal capacitance performance. We employed the areal capacitance value expressed in (F/cm^2) because it is a very important indicator of the performance of a supercapacitor and for its potential use as an electrode device.[49−56]

From Table 1, it can be seen that the 3D-NSE shows a highly competitive energy storage areal capacity, compared with other silver-based electrodes reported in previous publications.[51−55] Additionally, the 3D-NSE shows stable long-term electrochemical performance and cycle stability. Also, a bending cycle test was performed to demonstrate the mechanical stability of the fabricated electrode. Therefore, all of the above allows us to state that the 3D-NSE exhibits an ideal nanostructure with a high electrochemical performance and long-term stability, without the degradation of its mechanical structure.

Table 2 lists the specific capacitance values versus the voltage window at the current density of 6.4 mA/cm^2,

Table 2. Specific Capacitance Values for 3D-NSE versus the Voltage Window (ΔV) at a Current Density of 6.4 mA/cm^2

ΔV (V)	C (F/cm^2)
1.2	0.5
1	0.3
0.8	0.2

appreciating the existing linear relationship between the areal capacitance and cell voltage window for the 3D-NSE, where the areal capacitance values increase by increasing the voltage window due to the pseudocapacitance effect contribution to the entire capacitance, which is a typical phenomenon in pseudocapacitors.[76]

Considering the potential applications of this novel 3D nanostructured silver electrode, its leakage current and self-discharge values were both measured in a three-electrode electrochemical cell (Figure 7). The leakage current was measured at a constant voltage of 0.7 V for 2 h through an electrochemical cell. The obtained data shown in Figure 7a indicate that first, the leakage current drops rapidly to gradually stabilize and to reach a value close to 0.07 mA. Such a low leakage current value indicates an optimal capacitor performance,[77] which could be attributed to few shuttle reactions caused by the impurities in electrode materials.[78,79]

On the other hand, self-discharge of a supercapacitor refers to the gradual decrease in the voltage across the supercapacitor that occurs when the supercapacitor device is left in an open circuit. Therefore, self-discharge may reflect the efficiency that can be present in a supercapacitor as an energy storage device.[78] The self-discharge profile of the 3D-NSE obtained under an open-circuit voltage condition is shown in Figure 7b. As can be observed in the inset of Figure 7b, the 3D-NSE maintains approximately 50% of the initial charge potential

Table 1. Comparison of the 3D-NSE Characteristic Values with Other Silver-Based Electrodes Reported in Previous Publications

electrodes	electrolyte	current density	specific capacitance	cycle stability	reference
3D-NSE	5 M KOH	6.4 mA/cm^2	500 mF/cm^2	95% (2600[a])	this work
Ag/Cu_xO/CF-40	3 M KOH	2 mA/cm^2	1192 mF/cm^2	93.3% (10,000)	51
Ag/CNFs	6 M KOH	100 mA/cm^2	30.6 mF/cm^2	104% (10,000)	52
PANI/Ag/CNF aerogel	1 M H_2SO_4		176 mF/cm^2	-	53
Ag NWs/WO_3	1 M H_2SO_4		13.6 mF/cm^2	72.6% (5000)	54
Ag/Au/polypyrrole	-	5.8 mA/cm^2	0.58 mF/cm^2	93% (800)	55

[a]Bending cycles.

https://doi.org/10.1021/acsomega.3c02235
ACS Omega 2023, 8, 40087−40098

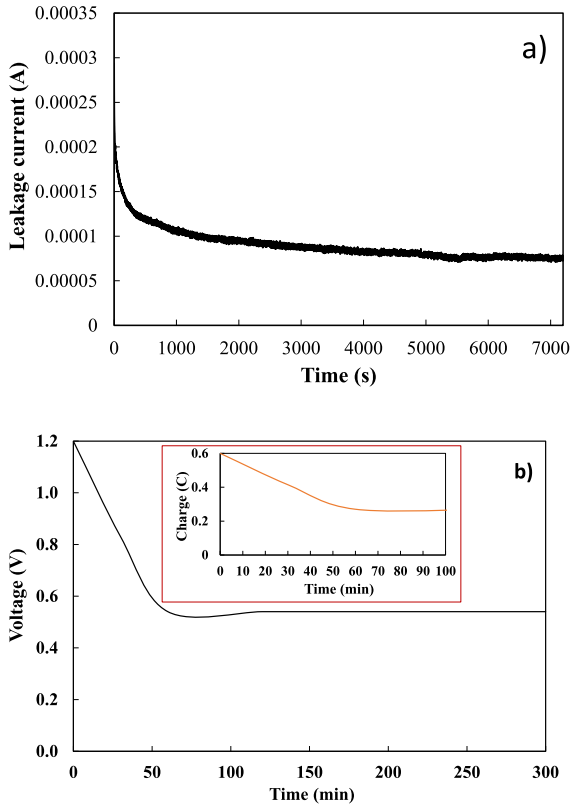

Figure 7. Leakage current curve for the 3D-NSE at a voltage value of 0.7 V and kept constant for 2 h (a). Self-discharge curve of the 3D-NSE under open-circuit conditions for 5 h after being charged at a voltage value of 0.7 V and the variation in the charge during the self-discharge process (inset) (b).

after 60 min of the self-discharge process, suggesting that charge redistribution plays an important role, since most of the voltage reduction can be due to the redistribution of charge carriers deep inside the holes of pores during longtime discharging, which is very typical in pseudocapacitors. All these effects are reflected in the lack of the self-discharge rates diminishing with longer hold times.[80−82]

Other important parameters for the performance characterization of a capacitor device are related to its energy density (E_d) and power density (P_d) values. The energy-storage performance for our 3D-NSE was evaluated from the Ragone plot shown in Figure 8. Noticeably, we obtained for the 3D-NSE an energy density value of 385.87 μWh/cm^2 (eq 6) at the

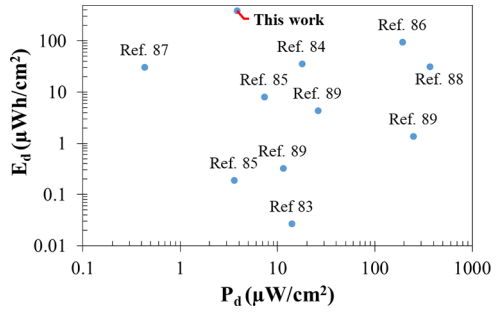

Figure 8. Ragone plot showing the classification of the 3D-NSE in comparison to previously reported electrodes used for supercapacitor applications.

power density of 3.82 μW/cm^2 (eq 7). The obtained values of areal energy and power densities for our 3D-NSE are very competitive, if we compare them with the previous ones reported for other types of electrodes used for supercapacitor applications.[83−89] Considering all these results, it is observed that the capacitance behavior of our 3D-NSE provides superior energy density performance as compared to EDLC capacitors because the Faradaic process occurs not only on the surface but also inside of these electrodes. Thus, on the pseudocapacitive materials, it is very important to design and synthesize a nanostructure that provides improved access to these reaction centers and shortens the ion diffusion lengths. All of these justify that the peculiar nanostructured design featured by our 3D-NSE would be especially appropriate for improving the redox charge-transfer process that occurs inside of the electrode, decreasing the electronic diffusion distances, which causes the 3D-NSE to have relatively large energy densities as compared to the previously reported silver electrodes.

At the same time, this behavior provides a lower power density because these faradaic processes are normally slower than nonfaradaic processes, which are associated with the intrinsic character of the electrochemical reactions that take place in these types of electrodes.[90,91] In addition, hybrid supercapacitors with an asymmetrical electrode configuration (where one electrode can be an electrostatic carbon material and the other one can be a faradaic capacitance material) begin to wake up a huge interest in numerous research investigations to capitalize on both electrode materials' advantages for improving the overall cell voltage, energy, and power densities.[92]

3.3. Electrochromoactive Behavior of 3D-NSEs.

Finally, we also analyze the electrochromoactive behavior of the fabricated 3D-NSE. Figure 9 shows the corresponding

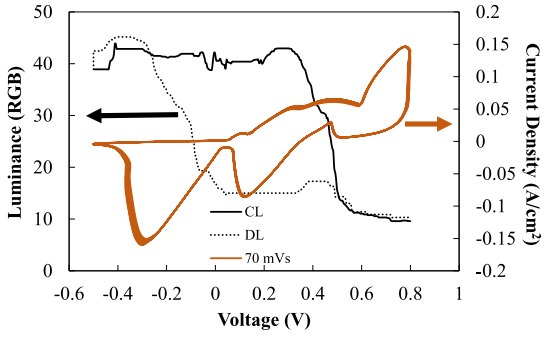

Figure 9. Electrochromoactive behavior exhibited by the 3D-NSE during the measurement taken at cyclic voltammetry for a scan rate of 70 mV/s.

color change experienced by the 3D-NSE during a cyclic voltammetry measurement taken at a scan rate of 70 mV/s. The obtained data indicate that the luminance of the device decreases (the electrode gets darker) as the 3D-NSE is charged (CL). On the other hand, when the 3D-NSE is discharged, the luminance increases (DL), which implies that the electrode is getting brighter, acquiring a grayish color. Therefore, the color changes of the electrode reflect the charging/discharging state of the 3D-NSE. It is because the color change, which takes place during the cycles of the charging/discharging process, is associated with the different silver oxides formed during the redox process exhibited by the 3D-NSE.[93]

https://doi.org/10.1021/acsomega.3c02235
ACS Omega 2023, 8, 40087−40098

Additionally, the video supported in the Supporting Information displays the electrochromoactive behavior exhibited by the 3D-NSE during one cycle of the charge/discharge operation mode. For all of these reasons, this nanostructured Ag electrode could be considered like a smart material because it reacts to external stimuli, such as the electric field, changing its optical properties, given that its color changed during the capacitor performance (see video in Supporting Information). Furthermore, this fabulous quality can also be used to test the correct electrode operation because the visual effect of color change is related with the electrical charge storage through the fast and reversible redox reactions and, therefore, is a direct indicator that the electrode is properly operating.[94,95]

Overall, this work is technologically very inspiring and represents the significant progress in achieving a high areal specific capacitance in an electrode film with several microns of thickness, which provides a nice manifestation on how to optimize the fundamental electrochemistry process (redox reaction, charge diffusion, etc.) by properly tailoring the electrode architecture.[96−98]

4. CONCLUSIONS

These experimental results reveal the feasibility to fabricate a metallic 3D-NSE with improved electrochemical properties for outstanding supercapacitor devices through facile and cost-effective template-assisted antireplica/replica processing. Its electrochemical performance as a supercapacitor electrode was systematically investigated, exhibiting a high areal capacitance value of 0.5 F cm^{-2} and a good Coulombic efficiency (97.5%). In addition, the 3D-NSE exhibits excellent capacitance retention (95%) after 2600 cycles at a current density of 6.4 mA cm^{-2}, indicating a good cyclic stability due to the excellent reversibility exhibited by this 3D nanostructured Ag electrode. Along with this, the 3D-NSE delivers a high energy density of around 385.87 μWh/cm^2 at a power density of 3.82 μW/cm^2 and also displays an electrochromoactive behavior. Furthermore, we have demonstrated that this nanostructured Ag electrode exhibits excellent electrochemical performance, such as high areal capacitance, increased energy density, and power density, as well as long and stable cycle life, together with added electrochromoactive behavior, which proves its suitability as an advanced electrode material for pseudosupercapacitor applications. Considering the results reported in this work, the fabricated nanopatterned metallic 3D-NSE can be considered as a very promising material for its implementation in novel energy storage systems such as micro-supercapacitors or in electrochemical devices.

■ ASSOCIATED CONTENT

Supporting Information

The Supporting Information is available free of charge at https://pubs.acs.org/doi/10.1021/acsomega.3c02235.

> Electrochromoactive behavior exhibited by the 3D-NSE during one cycle of charge/discharge operational mode. It also appreciates the visual effect of color change related with the electrical charge storage through fast and reversible redox reactions, which indicates that the 3D-NSE is properly operating (MP4)

■ AUTHOR INFORMATION

Corresponding Author

Victor M. Prida − *Depto. de Física, Facultad de Ciencias, Universidad de Oviedo, 33007 Oviedo, Spain;* orcid.org/0000-0001-5541-8816; Email: vmpp@uniovi.es

Authors

Ana Silvia González − *Depto. de Física, Facultad de Ciencias, Universidad de Oviedo, 33007 Oviedo, Spain*

Javier García − *Depto. de Física, Facultad de Ciencias, Universidad de Oviedo, 33007 Oviedo, Spain*

Victor Vega − *Laboratorio de Membranas Nanoporosas, Servicios Científico-Técnicos, Universidad de Oviedo, 33006 Oviedo, Spain*

Rafael Caballero Flores − *Depto. Física de la Materia Condensada, Facultad de Física, Universidad de Sevilla, 41080 Sevilla, Spain*

Complete contact information is available at: https://pubs.acs.org/10.1021/acsomega.3c02235

Author Contributions

The manuscript was written through contributions of all authors. All authors have given approval to the final version of the manuscript.

Funding

Spanish MCINN research grant no. PID2019−108075RB-C32/AEI/10.13039/501100011033. Regional government of Principado de Asturias under FICYT project ref.: SV-PA-21-AYUD/2021/51399.

Notes

The authors declare no competing financial interest.

■ ACKNOWLEDGMENTS

This work was supported by Spanish MCINN under research grant no. PID2019-108075RB-C32/AEI/10.13039/501100011033. The authors thank FICyT from Principado de Asturias for the financial support under project SV-PA-21-AYUD/2021/51399 and particularly A.S.G. for her research contract. The authors also wish to thank Dr. A. Castro-Muñiz (INCAR-CSIC) for his scientific and technical support on the 3D-NSE characterization.

■ REFERENCES

(1) Zhong, Y.; Xia, X.; Mai, W.; Tu, J.; Fan, H. J. Integration of Energy Harvesting and Electrochemical Storage Devices. *Adv. Mater. Technol.* **2017**, *2* (12), No. 1700182.

(2) Karthikeyan, S.; Narenthiran, B.; Sivanantham, A.; Bhatlu, L. D.; Maridurai, T. Supercapacitor: Evolution and Review. *Mater. Today: Proc.* **2021**, *46* (9), 3984−3988.

(3) Forouzandeh, P.; Kumaravel, V.; Pillai, S. C. Electrode Materials for Supercapacitors: A Review of Recent Advances. *Catalysts* **2020**, *10* (9), 969.

(4) Kumar, Y.; Rawal, S.; Joshi, B.; Hashmi, S. A. Background, Fundamental Understanding and Progress in Electrochemical Capacitors. *J. Solid. State. Electrochem.* **2019**, *23*, 667−692.

(5) Sung, J.; Shin, C. Recent Studies on Supercapacitors with Next-Generation Structures. *Micromachines* **2020**, *11* (12), 1125.

(6) Banerjee, S.; De, B.; Sinha, P.; Cherusseri, J.; Kar, K. K. *Applications of Supercapacitors in Handbook of Nanocomposite Supercapacitor Materials I*; Kar, K. K., Ed.; Springer Cham: Germany, 2020; pp 341−350.

(7) Wu, C.; Cai, J.; Zhang, Q.; Zhou, X.; Zhu, Y.; Shen, P. K.; Zhang, K. Hierarchical Mesoporous Zinc−Nickel−Cobalt Ternary Oxide Nanowire Arrays on Nickel Foam as High-Performance Electrodes for

Supercapacitors. *ACS Appl. Mater. Interfaces* **2015**, *7* (48), 26512−26521.
(8) Meng, Q.; Qin, K.; Ma, L.; He, C.; Liu, E.; He, F.; Shi, C.; Li, Q.; Li, J.; Zhao, N. N-Doped Porous Carbon Nanofibers/Porous Silver Network Hybrid for High-Rate Supercapacitor Electrode. *ACS Appl. Mater. Interfaces* **2017**, *9* (36), 30832−30839.
(9) Kumar, K. S.; Choudhary, N.; Jung, Y.; Thomas, J. Recent Advances in Two-Dimensional Nanomaterials for Supercapacitor Electrode Applications. *ACS Energy Lett.* **2018**, *3* (2), 482−495.
(10) Schlicht, S.; Büttner, P.; Bachmann, J. Highly Active Ir/TiO_2 Electrodes for the Oxygen Evolution Reaction Using Atomic Layer Deposition on Ordered Porous Substrates. *ACS Appl. Energy Mater.* **2019**, *2* (3), 2344−2349.
(11) Vu, V.-P.; Mai, V.-D.; Nguyen, D. C. T.; Lee, S.-H. Flexible and Self-Healable Supercapacitor with High Capacitance Restoration. *ACS Appl. Energy Mater.* **2022**, *5* (2), 2211−2220.
(12) Sharma, V.; Singh, I.; Chandra, A. Hollow Nanostructures of Metal Oxides as Next Generation Electrode Materials for Supercapacitors. *Sci. Rep.* **2018**, *8*, 1307.
(13) An, C.; Zhang, Y.; Guo, H.; Wang, Y. Metal Oxide-Based Supercapacitors: Progress and Prospectives. *Nanoscale Adv.* **2019**, *1*, 4644−4658.
(14) Makgopa, K.; Bello, A.; Raju, K.; Modibane, K. D.; Hato, M. J. Nanostructured Metal Oxides for Supercapacitor Applications. In *Emerging Nanostructured Materials for Energy and Environmental Science. Environmental Chemistry for a Sustainable World*; Springer International Publishing, chapter 6, 2019.
(15) Yuksel, R.; Coskun, S.; Kalay, Y. E.; Hunalan, H. E. Flexible, Silver Nanowire Network Nickel Hydroxide Core-Shell Electrodes for Supercapacitors. *J. Power Sources* **2016**, *328*, 167−173.
(16) Oje, A. I.; Ogwu, A. A.; Mirzaeian, M.; Oje, A. M.; Tsendzughul, N. Silver thin film electrodes for supercapacitor application. *Appl. Surf. Sci.* **2019**, *488*, 142−150.
(17) Ai, Y.; Lou, Z.; Li, L.; Chen, S.; Park, H. S.; Wang, Z. M.; Shen, G. Meters-Long Flexible $CoNiO_2$-Nanowires@Carbon-Fibers Based Wire-Supercapacitors for Wearable Electronics. *Adv. Mater. Technol.* **2016**, *1* (8), No. 1600142.
(18) Kate, R. S.; Khalate, S. A.; Deokate, R. J. Overview of Nanostructured Metal Oxides and Pure Nickel Oxide (NiO) Electrodes for Supercapacitors: A Review. *J. Alloys Compd.* **2018**, *734*, 89−111.
(19) Ke, S.-H.; Guo, P.-W.; Pang, C.-Y.; Tian, B.; Luo, C.-S.; Zhu, H.-P.; Wu, W. Screen-Printed Flexible Strain Sensors with Ag Nanowires for Intelligent and Tamper-Evident Packaging Applications. *Adv. Mater. Technol.* **2020**, *5* (5), No. 1901097.
(20) Sambasivam, S.; Raghavendra, K. V. G.; Yedluri, A. K.; Arbi, H. M.; Narayanaswamy, V.; Gopi, C. V. V. M.; Choi, B.-C.; Kim, H.-J.; Alzahmi, S.; Obaidat, I. M. Facile Fabrication of $MnCo_2O_4$/NiO Flower-Like Nanostructure Composites with Improved Energy Storage Capacity for High-Performance Supercapacitors. *Nanomaterials* **2021**, *11*, 1424.
(21) Wang, G.; Liu, Z.; Ma, C.; Du, Z.; Liu, D.; Cheng, K.; Ye, X.; Liu, T.; Bai, L. Engineering a Novel $AgMn_2O_4$@$Na_{0.55}Mn_2O_4$ Nanosheet toward High-Performance Electrochemical Capacitors. *Nanomaterials* **2022**, *12* (9), 1538.
(22) Fu, D.; Yang, R.; Wang, Y.; Wang, R.; Hua, F. Silver Nanowire Synthesis and Applications in Composites: Progress and Prospects. *Adv. Mater. Technol.* **2022**, *7*, No. 2200027.
(23) Tang, L.; Duan, F.; Chen, M. Silver nanoparticle decorated polyaniline/multiwalled super-short carbon nanotube nanocomposites for supercapacitor applications. *RSC Adv.* **2016**, *6*, 65012−65019.
(24) Shao, Y.; Wang, H.; Zhang, Q.; Li, Y. High-performance flexible asymmetric supercapacitors based on 3D porous graphene/MnO_2nanorod and graphene/Ag hybrid thin-film electrodes. *J. Mater. Chem. C* **2013**, *1*, 1245−1251.
(25) Patil, D. S.; Pawar, S. A.; Kim, J. H.; Patil, P. S.; Shin, J. C. Facile Preparation and Enhanced Capacitance of the Ag-PEDOT:PSS/Polyaniline Nanofiber Network for Supercapacitors. *Electrochim. Acta* **2016**, *213*, 680−690.
(26) Li, Y.; Fu, H.; Zhang, Y.; Wang, Z.; Li, X. Kirkendall Effect Induced One-Step Fabrication of Tubular Ag/MnOx Nanocomposites for Supercapacitor Application. *J. Phys. Chem. C* **2014**, *118* (13), 6604−6611.
(27) Wu, J.; Li, Z.; Lin, Y. Porous NiO/Ag composite film for electrochemical capacitor application. *Electrochim. Acta* **2011**, *56* (5), 2116−2121.
(28) Huang, J.; Wu, H.; Cao, D.; Wang, G. Influence of Ag doped CuO nanosheet arrays on electrochemical behaviors for supercapacitors. *Electrochim. Acta* **2012**, *75*, 208−212.
(29) Wang, X.; Zhang, P.; Vongehr, S.; Tang, S.; Wang, Y.; Meng, X. Large-scale fabrication of porous bulk silver thin sheets with tunable porosity for high-performance binder-free supercapacitor electrodes. *RSC Adv.* **2015**, *5*, 45194−45200.
(30) Devarayan, K.; Park, J.; Kim, H.-Y.; Kim, B.-S. Facile green synthesis of silver nanodendrite/cellulose acetate thin film electrodes for flexible supercapacitors. *Carbohydr. Polym.* **2017**, *163*, 153−161.
(31) Oje, A. I.; Ogwu, A. A.; Mirzaeian, M.; Tsendzughul, N. Electrochemical energy storage of silver and silver oxide thin films in an aqueous NaCl electrolyte. *J. Electroanal. Chem.* **2018**, *829*, 59−68.
(32) Zhang, D.; Li, W.; Ye, R.; Guo, X.; Wang, S.; Wang, X.; Xiang, Q. A Facile Strategy for $ZnFe_2O_4$ Coating Preparing By Electrophoretic Deposition and its Supercapacitor Performances. *J. Mater. Sci.: Mater. Electron.* **2018**, *29*, 5454−5458.
(33) Robert, K.; Douard, C.; Demortière, A.; Blanchard, F.; Roussel, P.; Brousse, T.; Lethien, C. On Chip Interdigitated Micro-Supercapacitors Based on Sputtered Bifunctional Vanadium Nitride Thin Films with Finely Tuned Inter- and Intracolumnar Porosities. *Adv. Mater. Technol.* **2018**, *3* (7), No. 1800036.
(34) Li, D.; Liu, X.; Chen, X.; Lai, W.-Y.; Huang, W. A Simple Strategy towards Highly Conductive Silver-Nanowire Inks for Screen-Printed Flexible Transparent Conductive Films and Wearable Energy-Storage Devices. *Adv. Mater. Technol.* **2019**, *4* (8), No. 1900196.
(35) Zhao, H.; Lei, Y. 3D Nanostructures for the Next Generation of High-Performance Nanodevices for Electrochemical Energy Conversion and Storage. *Adv. Energy Mater.* **2020**, *10* (28), No. 2001460.
(36) Hassan, I. U.; Salim, H.; Naikoo, G. A.; Awan, T.; Dar, R. A.; Arshad, F.; Tabidi, M. A.; Das, R.; Ahmed, W.; Asiri, A. M.; Qurashi, A. A. Review on Recent Advances in Hierarchically Porous Metal and Metal Oxide Nanostructures as Electrode Materials for Supercapacitors and Non-Enzymatic Glucose Sensors. *J. Saudi Chem. Soc.* **2021**, *25*, No. 101228.
(37) Xu, P.; Li, X.; Yu, H.; Xu, T. Advanced Nanoporous Materials for Micro-Gravimetric Sensing to Trace-Level Bio/Chemical Molecules. *Sensors* **2014**, *14* (10), 19023−19056.
(38) Baig, N.; Kammakakam, I.; Falathabe, W. Nanomaterials: A Review of Synthesis Methods, Properties, Recent Progress, and Challenges. *Mater. Adv.* **2021**, *2*, 1821−1871.
(39) Zhao, H.; Wang, C.; Vellacheri, R.; Zhou, M.; Xu, Y.; Fu, Q.; Wu, M.; Grote, F.; Lei, Y. Self-Supported Metallic Nanopore Arrays with Highly Oriented Nanoporous Structures as Ideally Nanostructured Electrodes for Supercapacitor Applications. *Adv. Mater.* **2014**, *26*, 7654−7659.
(40) Brzózka, A.; Jeleń, A.; Brudzisz, A. M.; Marzec, M. M.; Sulka, G. D. Electrocatalytic Reduction of Chloroform it Nanostructured Silver Electrodes. *Electrochim. Acta* **2017**, *225*, 574−583.
(41) Kim, S.-I.; Lee, J.-S.; Ahn, H.-J.; Song, H.-K.; Jang, J.-H. Facile Route to an Efficient NiO Supercapacitor with a Three-Dimensional Nanonetwork Morphology. *ACS Appl. Mater. Interfaces* **2013**, *5* (5), 1596−1603.
(42) Padmanathan, N.; Selladurai, S.; Razeeb, K. M. Ultra-Fast Rate Capability of a Symmetric Supercapacitor with a Hierarchical Co_3O_4 Nanowire/Nanoflower Hybrid Structure in Non-Aqueous Electrolyte. *RSC Adv.* **2015**, *5*, 12700−12709.
(43) Lokhande, P. E.; Chavan, U. S.; Pandey, A. Materials and Fabrication Methods for Electrochemical Supercapacitors: Overview. *Electrochem. Energy Rev.* **2020**, *3*, 155−186.

https://doi.org/10.1021/acsomega.3c02235
ACS Omega 2023, 8, 40087−40098

(44) Masuda, H.; Fukuda, K. Ordered Metal Nanohole Arrays Made by a Two-Step Replication of Honeycomb Structures of Anodic Alumina. *Science* **1995**, *268* (5216), 1466−1468.
(45) Cuevas, A. L.; Martínez de Yuso, M. de V.; Vega, V.; González, A. S.; Prida, V. M.; Benavente, J. Influence of ALD Coating Layers on the Optical Properties of Nanoporous Alumina-Based Structures. *Coatings* **2019**, *9* (1), 43.
(46) Gonzalez, A. S.; Vega, V.; Caballero-Flores, R.; García, J.; Prida, V. M. Procedimiento de Obtención de Electrodos de Plata Nanoestructurados y Electrodos de Plata Nanoestructurados/New Nanostructured Electrodes for Supercapacitors. ES P202100061, 2021.
(47) Kim, S.-K.; Seok, H.-J.; Kim, D.-H.; Dong-Hyeok, C.; Nam, S.-J.; Kim, S.-C.; Kim, H.-K. Comparison of NiO_x Thin Film Deposited by Spin-Coating or Thermal Evaporation for Application as a Hole Transport Layer of Perovskite Solar Cells. *RSC Adv.* **2020**, *10*, 43847−43852.
(48) Vogt, E.; Węgrzynowicz, A.; Vogt, O.; Čablík, V. Application of krypton and nitrogen isotherms to characterisation of hydrophobized fine dispersional limestone material. *Adsorption* **2019**, *25*, 477−483.
(49) Sivakkumar, S. R.; Kim, W. J.; Choi, J. A.; MacFarlane, D. R.; Forsyth, M.; Kim, D. W. Electrochemical performance of polyaniline nanofibres and polyaniline/multi-walled carbon nanotube composite as an electrode material for aqueous redox supercapacitors. *J. Power Sources* **2007**, *171*, 1062−1068.
(50) Cheng, Q.; Tang, J.; Ma, J.; Zhang, H.; Shinya, N.; Qin, L.-C. Polyaniline-Coated Electro-Etched Carbon Fiber Cloth Electrodes for Supercapacitors. *J. Phys. Chem. C* **2011**, *115* (47), 23584−23590.
(51) Jiang, H.; Yan, X.; Miao, J.; You, M.; Zhu, Y.; Pan, J.; Wang, L.; Cheng, X. Super-conductive silver nanoparticles functioned three-dimensional Cu_xO foams as a high-pseudocapacitive electrode for flexible asymmetric supercapacitors. *J. Materiomics* **2021**, *7*, 156−165.
(52) Kim, Y. I.; Samuel, E.; Joshi, B.; Kim, M.-W.; Kim, T. G.; Swihart, M. T.; Yoon, S. S. Highly efficient electrodes for supercapacitors using silver-plated carbon nanofibers with enhanced mechanical flexibility and long-term stability. *J. Chem. Eng.* **2018**, *353*, 189−196.
(53) Zhang, X.; Lin, Z.; Chen, B.; Zhang, W.; Sharma, S.; Gu, W.; Deng, Y. Solid-state flexible polyaniline/silver cellulose nanofibrils aerogel supercapacitors. *J. Power Sources* **2014**, *246*, 283−289.
(54) Shen, L.; Du, L.; Tan, S.; Zang, Z.; Zhao, C.; Mai, W. Flexible electrochromic supercapacitor hybrid electrodes based on tungsten oxide films and silver nanowires. *Chem. Commun.* **2016**, *52*, 6296−6299.
(55) Moon, H.; Lee, H.; Kwon, J.; Suh, Y. D.; Kim, D. K.; Ha, I.; Yeo, J.; Hong, S.; Ko, S. H. Ag/Au/Polypyrrole Core-shell Nanowire Network for Transparent, Stretchable and Flexible Supercapacitor in Wearable Energy Devices. *Sci. Rep.* **2017**, *7*, 41981.
(56) Douard, C.; Athouël, L.; Brown, D.; Crosnier, O.; Rebmann, G.; Schilling, O.; Brousse, T. Electrode Design for MnO_2-Based Aqueous Electrochemical Capacitors: Influence of Porosity and Mass Loading. *Materials* **2021**, *14* (11), 2990.
(57) Nguyen, R. M. H.; Brown, M. S. Why You Should Forget Luminance Conversion and Do Something Better. *2017 IEEE Conference on Computer Vision and Pattern Recognition (CVPR)*: Honolulu, HI, USA, (21−26 July), 2017; pp 5920−5928.
(58) Fatemeh, K.; Javad, M. M.; Samaneh, K. The effect of silver nanoparticles on composite shear bond strength to dentin with different adhesion protocols. *J. Appl. Oral Sci.* **2017**, *25*, 367−373.
(59) Heidarpour, F.; Ghani, W. A. W. A. B. K.; Ahmadun, F. R. B.; Sobri, S.; Zargar, M.; Mozafari, M. R. Nano Silver-Coated Polypropylene Water Filter: I. Manufacture by Electron Beam Gun Using a Modified Balzers 760 Machine. *Dig. J. Nanomater. Biostruct.* **2010**, *5* (3), 787−796. https://chalcogen.ro/787_Heidarpour-mss1.pdf
(60) Fowsiya, J.; Madhumitha, G. Biomolecules Derived from Carissa edulis for the Microwave Assisted Synthesis of Ag_2O Nanoparticles: A Study Against *S. incertulas, C. medinalis and S. mauritia*. *J. Clust. Sci.* **2019**, *30*, 1243−1252.
(61) Schuettler, M. Electrochemical properties of platinum electrodes in vitro: comparison of six different surface qualities. *Annu. Int. Conf. IEEE Eng. Med. Biol. Soc.* **2007**, *2007*, 186−189.
(62) Spitzer, P.; Wunderli, S.; Maksymiuk, K.; Michalska, A.; Kisiel, A.; Galus, Z.; Tauber, G. Reference Electrodes for Aqueous Solutions. *In Handbook of Reference Electrodes*; Inzelt, G.; Lewenstam, A.; Scholz, F., Eds.; Springer: Berlin, Heidelberg, 2013, pp 77−143.
(63) Abd El Rehim, S. S.; Hassan, H. H.; Ibrahim, M. A. M.; Amin, M. A. Electrochemical Behaviour of a Silver Electrode in NaOH Solutions. *Monatsh. Chem./Chem. Monthly* **1998**, *129*, 1103−1117.
(64) Luo, H.; Ji, X.; Cheng, S. Investigation into the Electrochemical Behaviour of Silver in Alkaline Solution and the Influence of Au-Decoration Using Operando Raman Spectroscopy. *RSC Adv.* **2020**, *10*, 8453−8459.
(65) Zhao, C.; Ju, P.; Wang, S.; Zhang, Y.; Min, S.; Qian, X. One-Step Hydrothermal Preparation of TiO_2/RGO/$Ni(OH)_2$/NF Electrode with High Performance for Supercapacitors. *Electrochim. Acta* **2016**, *218*, 216−227.
(66) Zhang, L.; Gong, H. Unravelling the Correlation Between Nickel to Copper Ratio of Binary Oxides and their Superior Supercapacitor Performance. *Electrochim. Acta* **2017**, *234*, 82−92.
(67) Karaphun, A.; Chirawatkul, P.; Maensiri, S.; Swatsitang, E. Influence of calcination temperature on the structural, morphological, optical, magnetic and electrochemical properties of $Cu_2P_2O_7$ nanocrystals. *J. Sol-Gel Sci. Technol.* **2018**, *88*, 407−421.
(68) Nguyen, K.; Hoa, N. D.; Hung, C. M.; Le, D. T. T.; Duy, N. V.; Hieu, N. V. A comparative study on the electrochemical properties of nanoporous nickel oxide nanowires and nanosheets prepared by a hydrothermal method. *RSC Adv.* **2018**, *8*, 19449−19455.
(69) Huang, H.; Niederberger, M. Towards fast-charging technologies in Li^+/Na^+ storage: from the perspectives of pseudocapacitive materials and non-aqueous hybrid capacitors. *Nanoscale* **2019**, *11*, 19225−19240.
(70) Yang, Y.; Zeng, D.; Yang, S.; Gu, L.; Liu, B.; Hao, S. Nickel Cobaltite Nanosheets Coated on Metal-Organic Framework-Derived Mesoporous Carbon Nanofibers for High-Performance Pseudocapacitors. *J. Colloid Interface Sci.* **2019**, *534*, 312−321.
(71) Cui, J.; Cao, L.; Zeng, D.; Wang, X.; Li, W.; Lin, Z.; Zhang, P. Surface Characteristic Effect of Ag/TiO_2 Nanoarray Composite Structure on Supercapacitor Electrode Properties. *Scanning* **2018**, *2018*, 1−10.
(72) Dong, M.; Wang, Z.; Li, X.; Guo, H.; Wang, J. A Smart Architecture of Nickel-Cobalt Sulfide Nanotubes Assembled Nanoclusters for High-Performance Pseudocapacitor. *J. Alloys Compd.* **2018**, *765*, 505−511.
(73) Zhu, J.; Tang, S.; Wu, J.; Shi, X.; Zhu, B.; Meng, X. Wearable High-Performance Supercapacitors Based on Silver-Sputtered Textiles with $FeCo_2S_4$−$NiCo_2S_4$ Composite Nanotube-Built Multitripod Architectures as Advanced Flexible Electrodes. *Adv. Energy Mater.* **2017**, *7*, No. 1601234.
(74) Liu, W.; Niu, H.; Yang, J.; Cheng, K.; Ye, K.; Zhu, K.; Wang, G.; Cao, D.; Yan, J. Ternary Transition Metal Sulfides Embedded in Graphene Nanosheets as Both the Anode and Cathode for High-Performance Asymmetric Supercapacitors. *Chem. Mater.* **2018**, *30*, 1055−1068.
(75) Shao, X.; Zhu, Z.; Zhao, C.; Zhao, C.; Qian, X. Hierarchical FeS/RGO/FeS@Fe foil as high-performance negative electrode for asymmetric supercapacitors. *Inorg. Chem. Front.* **2018**, *5*, 1912−1922.
(76) Zhang, L.; Meng, Z.; Qi, Q.; Yan, W.; Lin, N.; Liu, X. Y. Aqueous supercapacitors based on carbonized silk electrodes. *RSC Adv.* **2018**, *8*, 22146−22153.
(77) Xiong, G.; Meng, C.; Reifenberger, R. G.; Irazoqui, P. P.; Fisher, T. S. Graphitic Petal Electrodes for All-Solid-State Flexible Supercapacitors. *Adv. Energy Mater.* **2014**, *4* (3), 1300515−1300524.
(78) He, P.; Huang, Q.; Huang, B.; Chen, T. Controllable Synthesis of Ni−Co−Mn Multi-Component Metal Oxides with Various Morphologies for High-Performance Flexible Supercapacitors. *RSC Adv.* **2017**, *7*, 24353−24358.

https://doi.org/10.1021/acsomega.3c02235
ACS Omega 2023, 8, 40087−40098

(79) Wang, Y.-Z.; Shan, X.-Y.; Wang, D.-W.; Cheng, H.-M.; Li, F. Mitigating Self-Discharge of Carbon-Based Electrochemical Capacitors by Modifying their Electric-Double Layer to Maximize Energy Efficiency. *J. Energy Chem.* **2019**, *38*, 214−218.
(80) Liu, T.; Pell, W. G.; Conway, B. E. Self-discharge and potential recovery phenomena at thermally and electrochemically prepared RuO_2 supercapacitor electrodes. *Electrochim. Acta* **1997**, *42*, 3541−3552.
(81) Andreas, H. A.; Black, J. M.; Oickle, A. A. Self-discharge in Manganese Oxide Electrochemical Capacitor Electrodes in Aqueous Electrolytes with Comparisons to Faradaic and Charge Redistribution Models. *Electrochim. Acta* **2014**, *140*, 116−124.
(82) Andreas, H. A. Self-Discharge in Electrochemical Capacitors: A Perspective Article. *J. Electrochem. Soc.* **2015**, *162*, A5047−A5053.
(83) Bae, J.; Song, M. K.; Park, Y. J.; Kim, J. M.; Liu, M.; Wang, Z. L. Fiber Supercapacitors Made of Nanowire-Fiber Hybrid Structures for Wearable/Flexible Energy Storage. *Angew. Chem., Int. Ed.* **2011**, *50*, 1683−1687.
(84) Ghosh, D.; Lim, J.; Narayan, R.; Kim, S. O. High Energy Density All Solid State Asymmetric Pseudocapacitors Based on Free Standing Reduced Graphene Oxide-Co_3O_4 Composite Aerogel Electrodes. *ACS Appl. Mater. Interfaces* **2016**, *31* (8), 22253−22260.
(85) Guo, R. S.; Chen, J. T.; Yang, B. J.; Liu, L. Y.; Su, L. J.; Shen, B. S.; Yan, X. B. In-Plane Micro-Supercapacitors for an Integrated Device on One Piece of Paper. *Adv. Funct. Mater.* **2017**, *27*, No. 1702394.
(86) Jeong, J. H.; Park, J. W.; Lee, D. W.; Baughman, R. H.; Kim, S. J. Electrodeposition of α-MnO_2/γ-MnO_2 on Carbon Nanotube for Yarn Supercapacitor. *Sci. Rep.* **2019**, *9*, 11271.
(87) Zhengpeng, Y.; Yuanheng, J.; Yutao, N.; Yong, Z.; Chunjing, Z.; Ping, L.; Meng, Z.; Qingwen, L. One-step wet-spinning assembly of twisting-structured graphene/carbon nanotube fiber supercapacitor. *J. Energy Chem.* **2020**, *51*, 434−441, DOI: 10.1016/j.jechem.2020.02.023.
(88) Saha, S.; Arole, K.; Radovic, M.; Lutkenhaus, J. L.; Green, M. J. Nanoscale. One-step hydrothermal synthesis of porous Ti3C2Tz MXene/rGO gels for supercapacitor applications. *Nanoscale* **2021**, *13*, 16543−16553.
(89) Hepel, M. Advances in micro-supercapacitors (MSCs) with high energy density and fast charge-discharge capabilities for flexible bioelectronic devices—A review. *Electrochem. Sci. Adv.* **2022**, *3*, No. e2100222.
(90) Wahab, Y. A.; Naseer, M. N.; Zaidi, A. A.; Umair, T.; Khan, H.; Siddiqi, M. M.; Javed, M. S. Super Capacitors in Various Dimensionalities: Applications and Recent Advancements. *Encyclopedia of Energy Storage, Elsevier* **2022**, 682−691.
(91) Rodríguez, J.; Navarrete, E.. *Ultracapacitors. Encyclopedia of Electrical and Electronic Power Engineering*; Elsevier, 2023; pp 198−205.
(92) Viswanathan, B. Chapter 13 − Supercapacitors. *Energy Sources* **2016**, 315−328. Elsevier
(93) Gaikwad, A. M.; Gallaway, J. W.; Desai, D.; Steingart, D. A. Electrochemical-Mechanical Analysis of Printed Silver Electrodes in a Microfluidic Device. *J. Electrochem. Soc.* **2011**, *158*, A154.
(94) Nwanya, A. C.; Offiah, S. U.; Amaechi, I. C.; Agbo, S.; Ezugwu, S. C.; Sone, B. T.; Osuji, R. U.; Maaza, M.; Ezema, F. I. Electrochromic and electrochemical supercapacitive properties of Room Temperature PVP capped $Ni(OH)_2$/NiO Thin Films. *Electrochim. Acta* **2015**, *171*, 128−141.
(95) Cai, G.; Wang, X.; Cui, M.; Darmawan, P.; Wang, J.; Eh, A. L.-S.; Lee, P. S. Electrochromo-Supercapacitor Based on Direct Growth of NiO Nanoparticles. *Nano Energy* **2015**, *12*, 258−267.
(96) Tian, X.; Jin, J.; Yuan, S.; Chua, C. K.; Tor, S. B.; Zhou, K. Emerging 3D-Printed Electrochemical Energy Storage Devices: A Critical Review. *Adv. Energy Mater.* **2017**, *7*, No. 1700127.
(97) Yao, B.; Chandrasekaran, S.; Zhang, J.; Xiao, W.; Qian, F.; Zhu, C.; Duoss, E. B.; Spadaccini, C. M.; Worsley, M. A.; Li, Y. Efficient 3D Printed Pseudocapacitive Electrodes with Ultrahigh MnO_2 Loading. *Joule* **2019**, *3* (2), 459−470.
(98) Fan, H. J. Pseudocapacitor Electrodes: Regular Pores Matter. *Joule* **2019**, *3* (2), 317−319.

https://doi.org/10.1021/acsomega.3c02235
ACS Omega 2023, 8, 40087−40098